

A transportable optical lattice clock at the National Time Service Center

De-Huan Kong(孔德欢), Zhi-Hui Wang(王志辉), Feng Guo(郭峰), Qiang Zhang(张强), Xiao-Tong Lu(卢晓同), Ye-Bing Wang(王叶兵), Hong Chang(常宏)

Citation: Chin. Phys. B . 2020, 29(7): 070602 . **doi:** 10.1088/1674-1056/ab9290
Journal homepage: http://cpb.iphy.ac.cn; http://iopscience.iop.org/cpb

What follows is a list of articles you may be interested in

Analysis of iris-loaded resonance cavity in miniaturized maser

Zu-Gen Guo(郭祖根), Yong Zhang(张勇), Tao Tang(唐涛), Zhan-Liang Wang(王战亮), Yu-Bin Gong(宫玉彬), Fei Xiao(肖飞), Hua-Rong Gong(巩华荣)

Chin. Phys. B . 2020, 29(5): 050601 . **doi:** 10.1088/1674-1056/ab7d98

Development of the integrated integrating sphere cold atom clock

Ming-Yuan Yu(于明圆), Yan-Ling Meng(孟艳玲), Mei-Feng Ye(叶美凤), Xin Wang(王鑫), Xin-Chuan Ouyang(欧阳鑫川), Jin-Yin Wan(万金银), Ling Xiao(肖玲), Hua-Dong Cheng(成华东), Liang Liu(刘亮)

Chin. Phys. B . 2019, 28(7): 070602 . **doi:** 10.1088/1674-1056/28/7/070602

Ramsey-coherent population trapping Cs atomic clock based on lin||lin optical pumping with dispersion detection

Peng-Fei Cheng(程鹏飞), Jian-Wei Zhang(张建伟), Li-Jun Wang(王力军)

Chin. Phys. B . 2019, 28(7): 070601 . **doi:** 10.1088/1674-1056/28/7/070601

Photonic generation of RF and microwave signal with relative frequency instability of 10^{-15}

Lu-Lu Yan(闫露露), Wen-Yu Zhao(赵文宇), Yan-Yan Zhang(张颜艳), Zhao-Yang Tai(邰朝阳), Pan Zhang(张攀), Bing-Jie Rao(饶冰洁), Kai Ning(宁凯), Xiao-Fei Zhang(张晓斐), Wen-Ge Guo(郭文阁), Shou-Gang Zhang(张首刚), Hai-Feng Jiang(姜海峰)

Chin. Phys. B . 2018, 27(3): 030601 . **doi:** 10.1088/1674-1056/27/3/030601

Clock-transition spectrum of ^{171}Yb atoms in a one-dimensional optical lattice

Chen Ning, Zhou Min, Chen Hai-Qin, Fang Su, Huang Liang-Yu, Zhang Xiao-Hang, Gao Qi, Jiang Yan-Yi, Bi Zhi-Yi, Ma Long-Sheng, Xu Xin-Ye

Chin. Phys. B . 2013, 22(9): 090601 . **doi:** 10.1088/1674-1056/22/9/090601

SPECIAL TOPIC — Ultracold atom and its application in precision measurement

A transportable optical lattice clock at the National Time Service Center*

De-Huan Kong(孔德欢)[1,2], Zhi-Hui Wang(王志辉)[3], Feng Guo(郭峰)[1,2], Qiang Zhang(张强)[1,2], Xiao-Tong Lu(卢晓同)[1,2], Ye-Bing Wang(王叶兵)[1], and Hong Chang(常宏)[1,2,†]

[1] *CAS Key Laboratory of Time and Frequency Primary Standards, National Time Service Center, Xi'an* 710600, *China*
[2] *School of Astronomy and Space Science, University of Chinese Academy of Sciences (CAS), Beijing* 100049, *China*
[3] *State Key Laboratory of Quantum Optics and Quantum Optics Devices, Institute of Opto-Electronics, Shanxi University, Taiyuan* 030006, *China*

(Received 20 February 2020; revised manuscript received 30 April 2020; accepted manuscript online 13 May 2020)

We report a transportable one-dimensional optical lattice clock based on ^{87}Sr at the National Time Service Center. The transportable apparatus consists of a compact vacuum system and compact optical subsystems. The vacuum system with a size of 90 cm×20 cm×42 cm and the beam distributors are assembled on a double-layer optical breadboard. The modularized optical subsystems are integrated on independent optical breadboards. By using a 230 ms clock laser pulse, spin-polarized spectroscopy with a linewidth of 4.8 Hz is obtained which is close to the 3.9 Hz Fourier-limit linewidth. The time interleaved self-comparison frequency instability is determined to be 6.3×10^{-17} at an averaging time of 2000 s.

Keywords: optical lattice clock, strontium atoms, spin-polarized spectra, instability

PACS: 06.30.Ft, 32.70.Jz, 37.10.Jk, 42.62.Eh **DOI:** 10.1088/1674-1056/ab9290

1. Introduction

At present, the uncertainty or instability of the atomic optical clocks[1,2] reaches 10^{-19}, which is better than the existing microwave clocks by nearly two orders of magnitude.[3–7] As one of the candidates for the next-generation time-frequency standard, atomic optical clocks have been developed in many laboratories.[1,8–12] The optical clocks can be used for high precision tests of fundamental physics constants,[13,14] chronometric leveling-based geodesy,[15] gravitational wave detection,[16] topological dark matter hunting,[17] frequency metrology, and timekeeping.[18]

Most of the optical clocks are confined in laboratories due to their complicated and bulky experimental apparatuses, which limit the application of the optical clocks in scientific research and engineering. Therefore, it is necessary to design and develop more compact and transportable optical clocks, which have not only low instability and uncertainty, but also high operation reliability under different conditions[19,20] to promote the comparison of clock signals, especially intercontinental comparison, more accurate and cost-effective than satellite link and long-distance optical fiber link. Furthermore, the development of transportable clocks is highly conducive to the research on space optical clocks.[21]

To date, a number of groups have demonstrated the transportable optical clocks. In 2014, the transportable boson ^{88}Sr optical lattice clock was developed by the Italian LENS team with a physical system size of less than 2.0 m^3, a systematic uncertainty of 7.0×10^{-15}, and an instability of $4.0 \times 10^{-15}/\tau^{1/2}$.[8] In 2017, the German Physikalisch-Technische Bundesanstalt realized a transportable ^{87}Sr optical lattice clock with systematic uncertainty of 7.4×10^{-17} and instability of $1.3 \times 10^{-15}/\tau^{1/2}$, while the entire experimental system was reduced to a size of 2.2 m×3 m×2.2 m.[22] In China, the Wuhan Institute of Physics and Mathematics of the Chinese Academy of Sciences developed a transportable calcium ion optical clock in 2016. The systematic uncertainty is 7.8×10^{-17} and the instability is $2.3 \times 10^{-14}/\tau^{1/2}$.[23]

Considered as one of the promising candidates for the redefinition of a second of the international system of units (SI), the strontium optical lattice clocks are constructed at the National Time Service Center.[11] So far, the stationary ^{87}Sr optical lattice clock has a frequency instability of 4.0×10^{-17} at an averaging time of 8000 s and uncertainty of 9.6×10^{-17}.[24–26] Based on the stationary ^{87}Sr optical lattice clock, we develop a transportable optical clock. In this paper, we introduce the progress of the transportable optical clock based on ^{87}Sr. First of all, we miniaturize the vacuum system. At the same time, all the sub-optical systems are modularized and fiber-coupled into the vacuum system so that every part can be easily moved. Then a spin-polarized clock transition spectroscopy with a narrow linewidth of 4.8 Hz is obtained. Furthermore, we realize

*Project supported by the National Natural Science Foundation of China (Grant Nos. 61775220 and 11803042), the Key Research Project of Frontier Science of the Chinese Academy of Sciences (Grant No. QYZDB-SSW-JSC004), and the strategic Priority Research Program of the Chinese Academy of Sciences (Grant No. XDB21030100).

†Corresponding author. E-mail: changhong@ntsc.ac.cn

© 2020 Chinese Physical Society and IOP Publishing Ltd

the closed-loop operation and measure the frequency instability using the time interleaved self-comparison method.

2. The transportable optical clock setup

2.1. The vacuum system

The vacuum system mainly includes an atomic oven, a Zeeman slower, and a science chamber for the magneto-optical trap (MOT), as shown in Fig. 1(a), with a size of 90 cm $\times$20 cm$\times$42 cm.

The oven is heated to generate strontium atomic vapor. Then the atomic beam is high-collimated by a nozzle containing 50 capillaries (length: 15 mm, diameter: 0.2 mm). The atomic flux of the thermal atomic beam is about 5×10^{11} atoms/s at the oven temperature of 733 K. The atomic beam propagates along a homemade Zeeman slower which consists of eight independent coils with an approximately effective length of 18 cm.[27] With the combination of the Zeeman slowing laser and the Zeeman compensating magnetic field, the atomic velocity is reduced to a couple of tens meters per second. A sapphire window, which can prevent strontium vapor coating, is used for coupling the Zeeman slowing laser into the Zeeman slower effectively. The oven region and the MOT region are pumped by two ion pumps at speeds of 25 L/s and 45 L/s, respectively. During clock operation, the pressure in the oven region is 3.6×10^{-6} Pa and that in the MOT is 1.9×10^{-7} Pa.

The decelerated atomic beam is trapped by standard MOT technique at the center of the science chamber with fourteen CF16 optical windows, as shown in Fig. 1(a). The diameter of the chamber is 18 cm. The quadrupole magnetic field in the MOT is generated by a pair of anti-Helmholtz coils. The coils have a radius of 64 mm and are winded by copper wires with a diameter of 1.5 mm. The distance between the two coils is 25 mm. An axial gradient magnetic field of 46 G/cm is obtained when the coils are supplied with 12 A current.

Figure 1(b) shows the layout of the vacuum system placed on a double-layer transportable breadboard. The vacuum system is mounted on the upper layer. Beam distributors for both first-stage and second-stage MOTs are built on the bottom layer. The whole double-layer transportable device has a size of 100 cm$\times$50 cm$\times$60 cm.

The experimental arrangement for all laser beams coupled into the MOT is depicted in Fig. 1(c). The 461 nm trapping beams, the 689 nm trapping and stirring beams, the 679 nm and 707 nm repumping beams pass through the science chamber doubly. The 813 nm lattice beam is spatially overlapped with the atomic cloud to load atoms. The 698 nm clock laser passes through the chamber singly and excites atoms to obtain the clock transition spectrum. The polarized laser at 689 nm passes through the chamber singly in the gravity direction. A photomultiplier tube (PMT, H11526-20-NF, Hamamatsu) and an electron multiplying charge-coupled device (EMCCD, DU-897, Andor) are used for fluorescence detection in the orthogonal direction of the detecting laser beam to minimize the background noise.

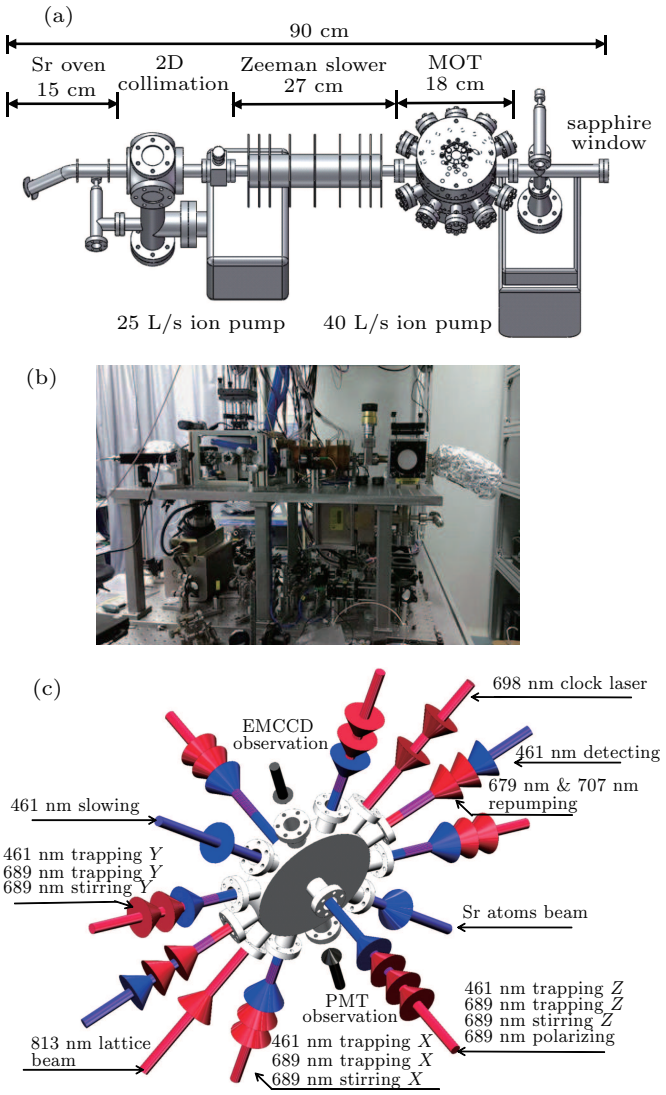


Fig. 1. (a) Technical drawing of the design of the vacuum system. (b) Layout of the vacuum system. (c) Experimental arrangement of all laser beams. EMCCD: electron multiplying charge-coupled device, PMT: photomultiplier tube.

2.2. Laser systems

To prepare atomic samples, the first stage cooling, the second stage cooling, and subsequent optical trapping in a one-dimensional (1D) lattice are performed.[11] To achieve the spectroscopy of the clock transition, the atoms are interrogated by a clock laser. Laser sources of six different wavelengths are used for the transportable optical clock according to the energy level structure of ^{87}Sr.[11] The involved laser subsystems are miniaturized and modularized as follows.

2.2.1. The first stage cooling laser system

In the first stage cooling, the atoms are three-dimensional magneto-optical trapped with the transition of $(5s^2)^1S_0(F=$

$9/2$)–$(5s5p)^1P_1(F = 11/2)$ corresponding to a wavelength of 461 nm. But the transition is not perfectly closed. In order to improve the efficiency of the first stage cooling, repumping lasers at 707 nm and 679 nm corresponding to the transitions of $(5s5p)^3P_2$–$(5s6s)^3S_1$ and $(5s5p)^3P_0$–$(5s6s)^3S_1$ are used to pump the atoms to the $(5s5p)^3P_1$ state, in which the atoms finally decay to the ground state.

A frequency-doubled 600 mW 461 nm laser (SHG-pro, Toptica) is employed in this stage. Figure 2(a) shows the schematic of the 461 nm laser system. The output of the 461 nm laser is divided into five parts for frequency locking, two-dimensional (2D) collimation, Zeeman slowing, trapping, and detecting with detunings of 51.8 MHz, −48 MHz, −469 MHz, −25 MHz, and 0 MHz, respectively. The detuning is given by $\Delta = \omega_{\text{laser}} - \omega_{\text{atom}}$, where ω_{laser} is the frequency of every light and ω_{atom} is the frequency of resonance transition $(5s^2)^1S_0(F = 9/2)$–$(5s5p)^1P_1(F = 11/2)$ of ^{87}Sr. The laser frequency is locked to the $(5s^2)^1S_0$–$(5s5p)^1P_1$ transition of ^{88}Sr. The 2D collimating beam is split into two parts evenly, propagating along the horizontal and vertical directions. Each collimating beam with power of 50 mW is especially shaped to an elliptic spot with a size of 30 mm×10 mm to reduce the atomic beam's divergence angle effectively. In order to balance the radiation pressure, both the beams are retro-reflected. A 30 mW Zeeman slowing laser with a diameter of 12 mm is coupled into the Zeeman slower to decrease the velocity of the atomic beam from 360 m/s to 50 m/s. Three pairs of counter-propagating trapping beams with a total power of 27 mW and a diameter of 12 mm are sent to the science chamber. The detecting laser beam for the fluorescence spectroscopy with a diameter of 5 mm is power stabilized to 1.3 mW by a noise eater (NEL01/M, Thorlabs). Figure 2(b) is the layout of the 461 nm laser system with size of 90 cm×60 cm.

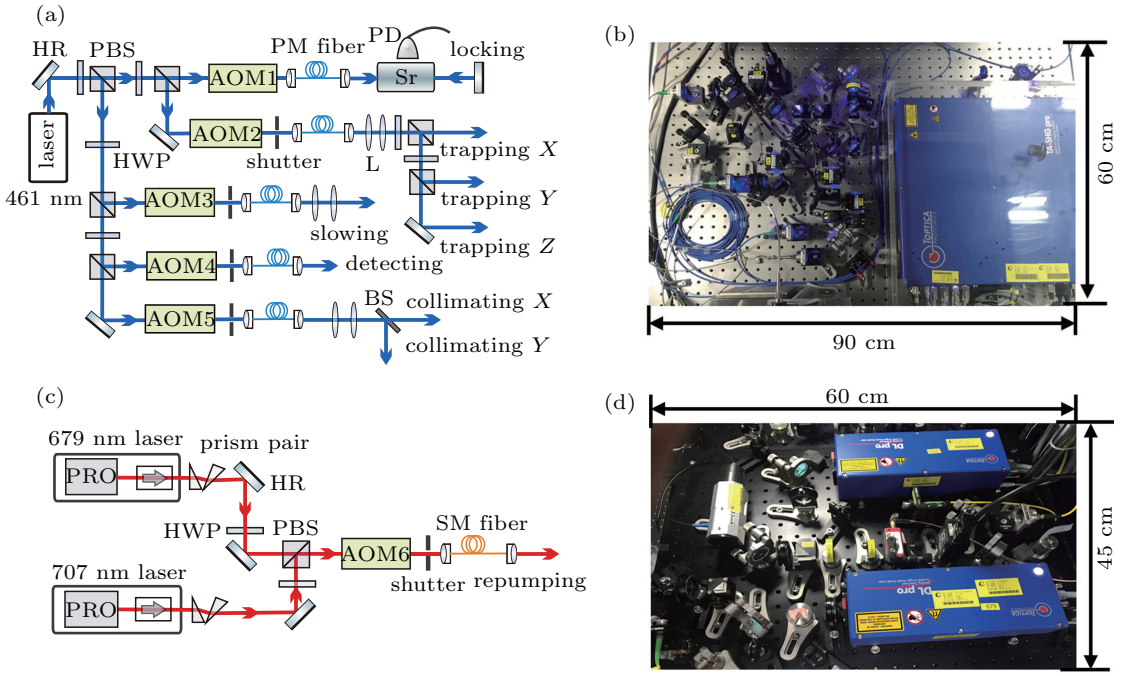


Fig. 2. Laser systems for the first cooling stage: (a) schematic and (b) layout of the 461 nm laser system setup; (c) schematic and (d) layout of the repumping laser system setup. HR: the mirror with high reflectivity; L: lens; HWP: half-wave plate; PBS: polarizing beam splitter; AOM: acousto-optic modulator; PD: photodetector; PM fiber: single-mode polarization-maintaining fiber; SM fiber: single-mode fiber.

Two external cavity diode lasers (ECDL) at 679 nm and 707 nm are employed as the repumping lasers. Figures 2(c) and 2(d) show schematic and layout of the repumping lasers, respectively. The 679 nm laser and the 707 nm laser beams are coupled into a single optical fiber after AOM6 (80 MHz). The output powers of the two lasers are 7 mW and 12 mW, respectively. In order to cover all hyperfine state transitions, the frequency of the 707 nm laser is scanned over 5 GHz.[11] The entire system is placed on a 60 cm×45 cm breadboard. In the experiment, the repumping beams with the same diameter of 15 mm are superimposed on the 461 nm detecting beam through a dichroic mirror. The number of atoms in the first-stage MOT is increased by a factor of 40 when adding the repumping lasers. After the 500 ms first-stage MOT, the diameter of the atomic cloud is about 1 mm with the number of 1.7×10^7 and a temperature of 5.1 mK measured by the time-of-flight (TOF) method.

2.2.2. The second stage of cooling laser system

For the second stage cooling, all the optical beams are produced in a compact module mainly containing a master laser and two slave lasers at 689 nm. The schematic of the 689 nm laser system is shown in Fig. 3(a). The master ECDL (Toptica) is frequency-locked to an ultralow-expansion (ULE) cubic cavity (Stable Laser Systems)[28] by using the Pound–Drever–Hall (PDH) technique. The length of the cubic cavity

is 25 mm and the zero crossing is 42.93 ℃. The fineness is calculated to be about 2×10^5 by measuring the ring-down spectroscopy. To evaluate the linewidth and instability, we employ heterodyne beating of the master laser with another narrow linewidth test laser at 689 nm locked on another ULE optical cavity with a finesse of 1.2×10^4. The linewidth of the master laser is approximately 163 Hz (full width at half maximum) by Lorentz fitting a heterodyne beat. The instability measured by the fractional Allan deviation is 1.6×10^{-14} at 1 s.

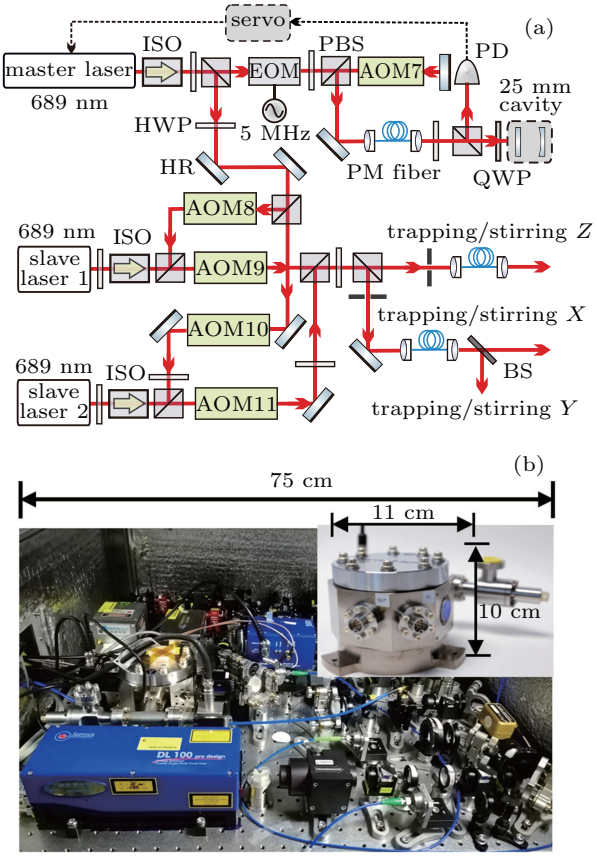


Fig. 3. (a) Schematic and layout of the second-stage cooling laser system. EOM: electro-optic modulator; AOM7–AOM11: acousto-optic modulator at 689 nm with frequency shifts of −2175 MHz, +520 MHz, +214 MHz, −520 MHz, −209 MHz; HR: high-reflectivity mirror; QWP: quarter-wave plate; HWP: half-wave plate; ISO: optical isolator; PBS: polarizing beam splitter; PD: photodetector; BS: beam splitter; PM fiber: single-mode polarization-maintaining fiber. (b) Layout of the second-stage cooling laser system. The insert in (b) is the vacuum chamber for the cubic cavity with a height of 10 cm and a diameter of 11 cm.

Utilizing the optical injection locking technique, the two slave lasers inherit the master laser's properties including linewidth and instability. We use a confocal Fabry–Perot cavity with a 1.5 GHz free spectral range and a finesse of 120 to monitor the single-longitudinal-mode operation condition of the slave lasers. The output from slave laser 1, modulated by AOM9, is used as trapping light corresponding to the inter-combination transition of $(5s^2)^1S_0(F = 9/2)$–$(5s5p)^3P_1(F = 11/2)$ of ^{87}Sr atoms. The slave laser 2, modulated by AOM11, is used as stirring light corresponding to the transition of $(5s^2)^1S_0(F = 9/2)$–$(5s5p)^3P_1(F = 9/2)$. The frequency difference between trapping light and stirring light is 1.46 GHz. The diameter of the 689 nm beams into the first-stage MOT is 10 mm. Figure 3(b) is the layout of the 689 nm laser system. The 75 cm×75 cm platform is covered with an acoustic-damping material enclosure. The vacuum chamber for the cubic cavity in the inset of Fig. 3(b) has a height of 10 cm and a diameter of 11 cm.

After the first stage cooling, the Zeeman slower is turned off and the MOT magnetic field gradient is reduced to 3 G/cm immediately. In order to cover a wide range of atomic velocities during the atom transfer process from the first-stage to the second-stage MOT, both wide line trapping and stirring laser beams for the second-stage MOT should be frequency-modulated at 50 kHz with a span of 3.4 MHz. The laser power is 2 mW for wide line trapping and stirring at each direction. In the wide line trapping and stirring phase of 100 ms, the MOT magnetic field gradient of 3 G/cm lasts for 10 ms and is linearly increased to 10 G/cm to compress the atomic cloud within 90 ms. Then we switch into the narrow line trapping and stirring to further reduce the temperature of the atomic clouds. The powers of each narrow line trapping beam and stirring beam are about 40 μW and 10 μW, respectively. The narrow line trapping and stirring last for 30 ms under the constant magnetic field gradient of 10 G/cm. The final transfer efficiency of atoms from the first-stage MOT to the second-stage MOT is approximately 10%. After the second stage of cooling, the atomic cloud has a size of about 0.6 mm with the number of 2.0×10^6 and a temperature of 4.4 μK.

2.2.3. Lattice laser and clock laser system

For the 1D optical lattice trapping, we use a 1 W diode laser at the magic wavelength of 813 nm (TA-pro, Toptica)[29] which is fixed on a 50 cm×45 cm breadboard. The lattice laser output is coupled into a single-mode polarization-maintaining fiber and focused into the center of the MOT with a 150 mm focus length lens. After reflected and shaped, the retro-reflected beam superposes with the incident beam to form a 1D lattice. The waist of the incident beam and retro-reflected beam is approximately 46 μm. In order to load atoms efficiently, the waist positions are overlapped with the atomic cloud exactly. When the power of the incident beam is 400 mW, the depth of the lattice is 21.1 μK, deep enough to trap atoms from the second-stage MOT. The experimental arrangement of the lattice trap is shown in Fig. 4. The lifetime of atoms trapped in the lattice is measured to be 600 ms.

In the opposite direction of the 813 nm laser beam is the 698 nm clock laser beam corresponding to the transition of $(5s^2)^1S_0(F = 9/2)$–$(5s5p)^3P_0(F = 9/2)$. The 698 nm ECDL (Toptica) is locked to a 10 cm ULE cavity with the finesse of 4×10^5 by the PDH method. The linewidth is approximately 1 Hz.[11] The 698 nm laser is delivered to the MOT by a 10 m

single-mode polarization-maintaining fiber. In Fig. 4, AOM12 is used to scan the frequency of the light and enable frequency feedback to match the transportable optical clock transition. The 698 nm beam is approximately collimated with a waist of 400 μm. The size of the 698 nm laser system is about 80 cm ×80 cm×25 cm.

Both polarizations of 698 nm clock laser and 813 nm lattice laser input into the MOT are purified as linear in gravity direction by using two Gran–Taylor prisms.

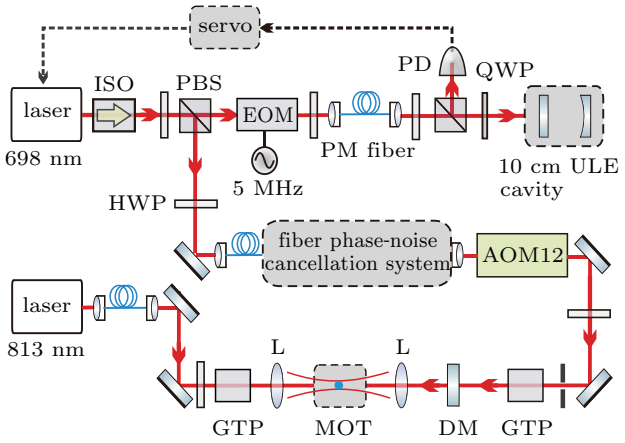


Fig. 4. Schematic of 813 nm and 698 nm experimental setup. EOM: electro-optic modulator; AOM12: acousto-optic modulator at 698 nm with a frequency shift of −410 MHz; QWP: quarter-wave plate; HWP: half-wave plate; ISO: optical isolator; PBS: polarizing beam splitter; PD: photodetector; GTP: Gran–Taylor prism; DM: dichroic mirror; L: lens with focus length of 150 mm; PM fiber: single-mode polarization-maintaining fiber.

3. Experimental results

3.1. Resolved sideband spectroscopy

After being loaded into the lattice, the atoms are interrogated by 698 nm clock laser with a pulse length of 80 ms and a power of 300 μW. We use a normalized electron-shelving detection technique[30] by applying a combination of 461 nm detecting light for atoms fluorescence on the ground state $^1S_0$ and repumping light to repump the excited atoms back to the ground state. Then we can get the normalized excitation fraction at the frequency of the interrogation laser. By scanning the frequency of the clock laser with steps of 300 Hz, the resolved sideband spectroscopy of the clock transition is obtained as shown in Fig. 5. The result indicates that the longitudinal trapping frequency of the lattice is approximately 68 kHz according to the frequency gap between the carrier and red sideband (or the blue sideband). The corresponding trap depth is about 20.8 μK consistent with the theoretical result. According to the area ratio of the blue sideband to the red sideband,[31] the temperature of the atoms is calculated as 3.3 μK in the longitudinal axis. Moreover, the linewidth of the carrier spectrum is 495 Hz by Lorentz fitting as shown in Fig. 5.

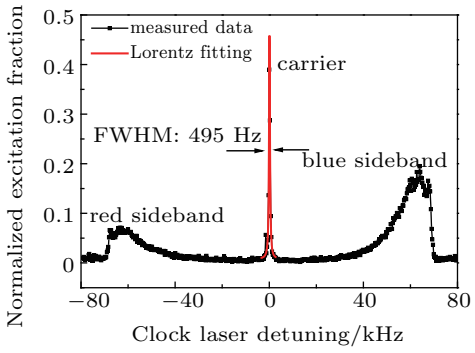


Fig. 5. Resolved sideband spectroscopy of the clock transition consisting of a narrow carrier peak in the center, red sideband, and blue sideband.

3.2. Spin-polarized spectra

Since ^{87}Sr has a nuclear spin $I = 9/2$, there are ten ground sublevel states. In order to increase the signal to noise ratio and excitation ratio, the atoms are pumped into stretched states of $m_F = +9/2$ or $m_F = -9/2$ using a weak polarized light in the direction of gravity. The frequency of the polarized light is resonant with transition $(5s^2)^1S_0(F = 9/2)$–$(5s5p)^3P_1(F = 9/2)$. During the spin polarization process, a group of three-dimensional compensating coils is turned on to remove the horizontal magnetic field and a weak bias magnetic field of about 100 mG is applied in the direction of gravity. Meanwhile, the 200 μW polarized light is turned on and lasts for 15 ms. The polarization of the polarized light is adjusted by a liquid crystal wave plate into $\sigma+$ or $\sigma-$, and the atoms are prepared into the stretched state of $m_F = +9/2$ or

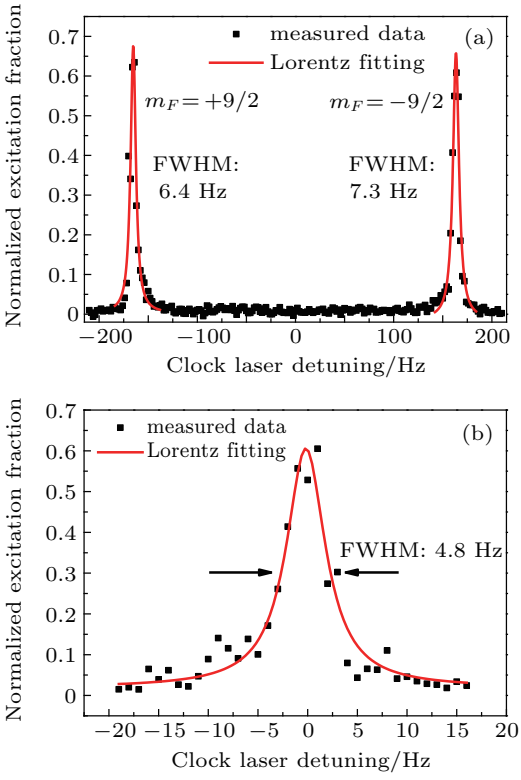


Fig. 6. (a) The measured spin-polarized spectra of the transitions from $m_F = +9/2$ to $m_F = +9/2$ and from $m_F = -9/2$ to $m_F = -9/2$. (b) Lorentz fitting (red solid) for the spin-polarized spectroscopy of the transition from $m_F = +9/2$ to $m_F = +9/2$ shows the linewidth of 4.8 Hz when the 698 nm interrogation time is 230 ms.

$m_F = -9/2$. After completing spin polarization, the bias magnetic field in the direction of gravity is increased to 330 mG to separate the ground sublevels. Furthermore, we perform spin-polarized spectra[32] using a 30 nW interrogation laser with 180 ms pulse length, as shown in Fig. 6(a). Lorentz fittings show that the linewidths are 6.4 Hz and 7.3 Hz for the spin-polarized spectra of the transitions from $m_F = +9/2$ to $m_F = +9/2$ and from $m_F = -9/2$ to $m_F = -9/2$, respectively. In order to achieve a narrower spin-polarized spectroscopy, the power of the interrogation laser is decreased to 10 nW and the pulse length is increased to 230 ms. The transition spectrum of $m_F = -9/2$ is achieved, as shown in Fig. 6(b). The linewidth of 4.8 Hz is obtained by Lorentz fitting, which is close to the Fourier limit of 3.9 Hz.

3.3. Frequency instability measured by self-comparison method

The time interleaved self-comparison method, usually employed to measure the systematic frequency shift, is used to verify the frequency stability improvement of the transportable optical clock.[33,34] Figure 7 shows the schematic of the time interleaved self-comparison measurement of the transportable optical clock. As shown in Fig. 7(a), the clock laser is modulated by AOM12. The radio frequency (RF) signal is supplied by an arbitrary function generator locked to an H-master (10 MHz). Two independent digital feedback loops servos A and B share the same spin-polarized spectroscopy of $(5s^2)^1S_0(F = 9/2, m_F = +9/2)$–$(5s5p)^3P_0(F = 9/2, m_F = +9/2)$ as reference and operate with the same experimental parameters. The servos A and B are compared in time interleaved way. The duration of each interleaved measurement cycle which includes four equal clock cycles is 4 s. For servo A, the difference between the measured excitation probability at half width points of the spin-polarized spectroscopy ($P_{1,A}$–$P_{2,A}$) gives the frequency error signal of the interrogation laser respect to the atomic transition in 1–2 clock cycles, as shown in Fig. 7(b). The error signal is fed into a digital proportional-integral differentiation (PID) filter to evaluate the correction frequency f_A that will be applied to the clock laser frequency for the next interrogation. For servo B ($P_{1,B}$–$P_{2,B}$), the error signal is obtained in 3–4 clock cycles. Another independent digital PID filter is employed to correct the f_B. The two correction frequencies f_A and f_B are fed back to the AOM12 alternately to keep in-loop operation. The difference between f_A and f_B is used for the evaluation of the frequency instability by the self-comparison measurement.

Figure 8 presents the Allan deviation by calculating the measured frequency differences. The differential frequency instability is 6.3×10^{-17} at an averaging time of 2000 s. The fitting shows that the time interleaved self-comparison frequency instability is $3.6 \times 10^{-15}/\tau^{1/2}$ affected mainly by white noise.

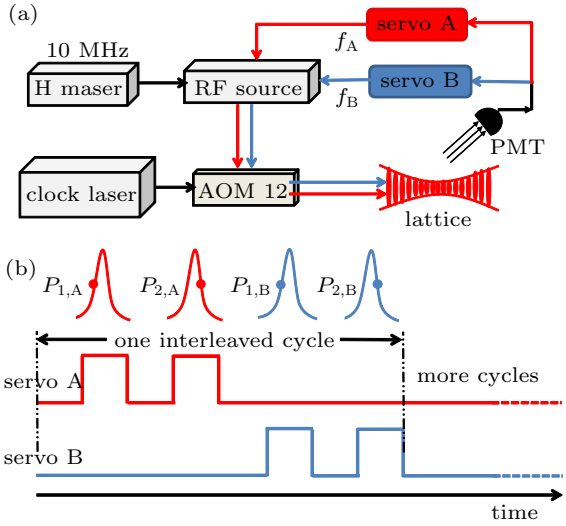


Fig. 7. Schematic diagram of the time interleaved self-comparison measurement method. (a) Two independent digital feedback loop servos A and B alternatively probe the clock transition. The two correction frequencies f_A and f_B are fed back to the AOM12 alternately to keep in-loop operation. (b) The timing sequence of instability measurement. Each interleaved measurement cycle contains 4 clock interrogation cycles and the period of the single clock probe cycle is 1 s.

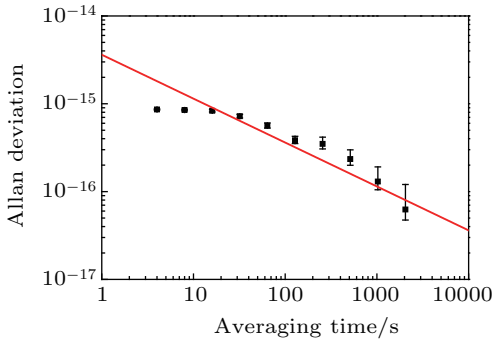


Fig. 8. Differential frequency instability evaluation of the transportable optical clock. The black solid squares show the Allan deviation of the time interleaved self-comparison measurements. The Allan deviation fits to $3.6 \times 10^{-15}/\tau^{1/2}$ (red solid line).

4. Conclusion and perspectives

In summary, we have constructed a miniaturized and modularized transportable optical clock. Compared with the traditional stationary optical clocks, the transportable optical clock has a more compact design. The volume of the vacuum system is reduced to 90 cm×20 cm×42 cm and all optical subsystems are integrated on independent optical breadboards. Apart from the electronics, the whole setup has been constructed within a size of 0.65 m^3. The spin polarization spectrum with a linewidth of 4.8 Hz is obtained, which serves as a reference for the closed-loop operation of the transportable optical clock. The frequency instability is $3.6 \times 10^{-15}/\tau^{1/2}$ and reaches 6.3×10^{-17} at an averaging time of 2000 s measured by the time interleaved self-comparison method. After completing the uncertainty evaluation and measurement of the absolute frequency of the clock transition in the next step, the

transportable optical clock is expected to perform frequency comparison with other clocks and precision measurement.

References

[1] Oelker E, Hutson R B, Kennedy C J, Sonderhouse L, Bothwell T, Goban A, Kedar D, Sanner C, Robinson J M, Marti G E, Matei D G, Legero T, Giunta M, Holzwarth R, Riehle F, Sterr U and Ye J 2019 *Nat. Photon.* **13** 714

[2] Brewer S M, Chen J S, Hankin A M, Clements E R, Chou C W, Wineland D J, Hume D B and Leibrandt D R 2019 *Phys. Rev. Lett.* **123** 033201

[3] Paul S, Swanson T B, Hanssen J and Taylor J 2017 *Metrologia* **54** 247

[4] Ludlow A D, Boyd M M, Ye J, Peik E and Schimidt P O 2015 *Rev. Mod. Phys.* **87** 637

[5] Nicholson T L, Campbell S L, Hutson R B, Marti G E, Bloom B G, MacNally R L, Zhang W, Barrett M D, Safronova M S, Strouse G F, Tew W L and Ye J 2015 *Nat. Commun.* **6** 6896

[6] Campbell S L, Hutson R B, Marti G E, Goban A, Darkwah Oppong N, MacNally R L, Souderhouse L, Robinson J M, Zhang W, Bloom B G and Ye J 2017 *Science* **358** 90

[7] Liu H, Zhang X, Jiang K L, Wang J Q, Zhou Q, Xiong Z X, He L X and Lyu B L 2017 *Chin. Phys. Lett.* **34** 020601

[8] Poli N, Schioppo M, Vogt S, Falke St, Sterr U, Lisdat Ch and Tino G M 2014 *Appl. Phys. B* **117** 1107

[9] Ohmae N, Sakama S and Katori H 2019 *Electr. Commun. Jpn.* **102** 43

[10] Lin Y G, Wang Q, Li Y, Meng F, Lin B K, Zang E J, Sun Z, Fang F, Li T C and Fang Z J 2015 *Chin. Phys. Lett.* **32** 090601

[11] Wang Y B, Yin M J, Ren J, Xu Q F, Lu B Q, Han J X, Guo Y and Chang H 2018 *Chin. Phys. B* **27** 023701

[12] Origlia S, Pramod M S, Schiller S, Singh Y, Bongs K, Schwarz R, Al-Masoudi A, Dörscher S, Häfner S, Sterr U and Lisdat Ch 2018 *Phys. Rev. A* **98** 053443

[13] Schiller S, Tino G M, Gill P, *et al.* 2009 *Exp. Astron.* **23** 573

[14] Wolf P, Bordé Ch J, Clairon A, *et al.* 2009 *Exp. Astron.* **23** 651

[15] Grotti J, Koller S, Vogt S, *et al.* 2014 *Nat. Phys.* **14** 437

[16] Kollwitz S, Pikovski I, Langellier N, Lukin M D, Walsworth R L and Ye J 2016 *Phys. Rev. D* **94** 124043

[17] Derevianko A and Pospelov M 2014 *Nat. Phys.* **10** 933

[18] Petit G, Arias F and Panfilo G 2015 *C. R. Phys.* **16** 480

[19] Fujieda M, Piester G, Gotoh T, Becker J, Aida M and Bauch A 2014 *Metrologia* **51** 253

[20] Takano T, Takamoto M, Ushijima I, Ohmae N, Akatsuka T, Yamaguchi A, Kuroishi Y, Munekane H, Miyahara B and Hidetoshi Katori 2016 *Nat. Photon.* **10** 662

[21] Mcgrew W F, Zhang X, Fasano R J, Schäffer S A, Beloy K, Nicolodi D, Brown R C, Hinkley N, Milani G, Schioppo M, Yoon T H and Ludlow A D 2018 *Nature* **564** 87

[22] Koller S B, Grotti J, Vogt S, Al-Masoudi A, Dörscher S, Häfner S, Sterr U and Lisdat Ch 2017 *Phys. Rev. Lett.* **118** 073601

[23] Cao J, Zhang P, Shang J, Cui K, Yuan J, Chao S, Wang S, Shu H and Huang X 2017 *Appl. Phys. B* **123** 112

[24] Lu X T, Li T, Kong D H, Wang Y B and Chang H 2019 *Acta Phys. Sin.* **68** 233401 (in Chinese)

[25] Li T, Lu X T, Zhang Q, Kong D H, Wang Y B and Chang H 2019 *Acta Phys. Sin.* **68** 093701 (in Chinese)

[26] Lu X T, Yin M J, Li T, Wang Y B and Chang H 2020 *Appl. Sci.* **10** 1440

[27] Han J X, Lu X T, Lu B Q, wang Y B, Kong D H, Zhang S G and Chang H 2018 *Acta Opt. Sin.* **38** 0702001

[28] Stephen W and Patrick G 2011 *Opt. Lett.* **36** 3572

[29] Ido T and Katori H 2003 *Phys. Rev. Lett.* **91** 053001

[30] Falke S, Schnatz H, Winfred J, Middlemann T, Vogt S, Weyer S, Lipphardt B, Grosche G, Riehle F, Sterr U and Lisdat C 2011 *Metrologia* **48** 399

[31] Blatt S, Thomsen J W, Campbell G K, Ludlow A D, Swallows M D, Martin M J, Boyd M M and Ye J 2009 *Phys. Rev. A* **80** 052703

[32] Guo Y, Yin M J, Xu Q F, Wang Y B, Lu B Q, Ren J, Zhao F J and Chang H 2018 *Acta Phys. Sin.* **67** 070601 (in Chinese)

[33] Li Y, Lin Y G, Wang Q, Yang T, Sun Z, Zang E J, Fang Z J 2018 *Chin. Opt. Lett.* **16** 051402

[34] Lin Y G and Fang Z J 2018 *Acta Phys. Sin.* **67** 160604 (in Chinese)